Molecular Therapy
Original Article

A Drug-Tunable Gene Therapy for Broad-Spectrum Protection against Retinal Degeneration

Clayton P. Santiago,[1] Casey J. Keuthan,[1] Sanford L. Boye,[1] Shannon E. Boye,[1] Aisha A. Imam,[1] and John D. Ash[1]

[1]Department of Ophthalmology, University of Florida, Gainesville, FL, USA

Retinal degenerations are a large cluster of diseases characterized by the irreversible loss of light-sensitive photoreceptors that impairs the vision of 9.1 million people in the US. An attractive treatment option is to use gene therapy to deliver broad-spectrum neuroprotective factors. However, this approach has had limited clinical translation because of the inability to control transgene expression. To address this problem, we generated an adeno-associated virus vector named RPF2 that was engineered to express domains of leukemia inhibitory factor fused to the destabilization domain of bacterial dihydrofolate reductase. Fusion proteins containing the destabilization domain are degraded in mammalian cells but can be stabilized with the binding of the drug trimethoprim. Our data show that expression levels of RPF2 are tightly regulated by the dose of trimethoprim and can be reversed by trimethoprim withdrawal. We further show that stabilized RPF2 can protect photoreceptors and prevent blindness in treated mice.

INTRODUCTION

Vision loss is often due to the death of neurons that either initiate the visual response to light (photoreceptors) or the neurons that transmit the signal to the brain (bipolar cells, ganglion cells, etc.).[1] As there are approximately 18 million people worldwide living with some form of retinal degenerating disease, this is a significant cause of morbidity in human health.[2] To date, mutations in approximately 250 genes have been identified to cause inherited retinal diseases.[3] For example, retinitis pigmentosa is a group of monogenetic diseases in which patients often have impaired night and peripheral vision beginning from childhood, which progressively worsens until central vision is lost.[4] Other retinal degenerative disorders, such as age-related macular degeneration (AMD), are caused by a multitude of factors, such as polymorphisms in complement factor H, obesity, smoking, and hypertension.[5–10] To address these diseases, many gene therapy strategies, including targeted gene replacement and gene editing, are under development.[11–15] However, it is a daunting task to design therapies for every individual gene or mutation that causes retinal dysfunction. To circumvent this challenge, additional strategies are based on gene or mutation-independent approaches, including expression of transcriptional regulators, inhibitors of apoptosis, regulators of oxidative defense, inhibitors of inflammation, and expression of neurotrophic factors, as well as interventions after cell death such as optogenetics and stem cell therapies.[16–26]

We, and others, have found that neuroprotective cytokines such as leukemia inhibitory factor (LIF) or ciliary neurotrophic factor (CNTF) can protect photoreceptors from a broad range of insults, including mechanical injury and multiple mutations that cause inherited retinal degeneration.[27–29] However, one problem with using LIF or CNTF as a gene therapy is that the long-term effects of highly expressed neurotrophic factors have been shown to be detrimental to retinal function and may promote inflammation.[30–32] What is needed to make these gene-independent approaches a viable therapy is a mechanism to control the level of transgene expression and the ability to turn it off, should adverse events occur.

Recently, drug-regulated destabilization domains have been shown to control transgene expression in the brain.[33–35] This system requires fusing the *E. coli* dihydrofolate reductase (DHFR) gene to the transgene of interest to produce a fusion protein. In mammalian cells, fusion proteins containing the DHFR protein are rapidly ubiquitinated and degraded by the proteasome system.[36,37] Because the DHFR portion of the fusion protein causes protein turnover, it is referred to as a destabilization domain (DD). The FDA-approved antibiotic trimethoprim (TMP) can bind to the DD and prevent the protein from being degraded, which allows the fusion protein to escape degradation.[33] Additionally, this antibiotic can cross the blood-brain barrier.[34,35]

In this study, we designed a neurotrophic factor-DD fusion protein that we have named Retinal Protective Factor 2 (RPF2). Our data demonstrate that TMP can be used to regulate RPF2 production *in vitro* and *in vivo* in a dose-dependent manner and that expression was reversible by TMP withdrawal. Moreover, we found that long-term treatment of RPF2 did not alter retinal function or morphology. Lastly, RPF2 treatment could rescue photoreceptors from an acute light-induced degeneration model, as well as preserve cone vision in the phosphodiesterase 6b mutant (*rd10*) inherited retinal degeneration model.

Received 1 April 2018; accepted 16 July 2018;
https://doi.org/10.1016/j.ymthe.2018.07.016.

Correspondence: John D. Ash, University of Florida, 1600 SW Archer Road, Academic Research Building R1-291, Gainesville, FL 32610, USA.
E-mail: jash@ufl.edu

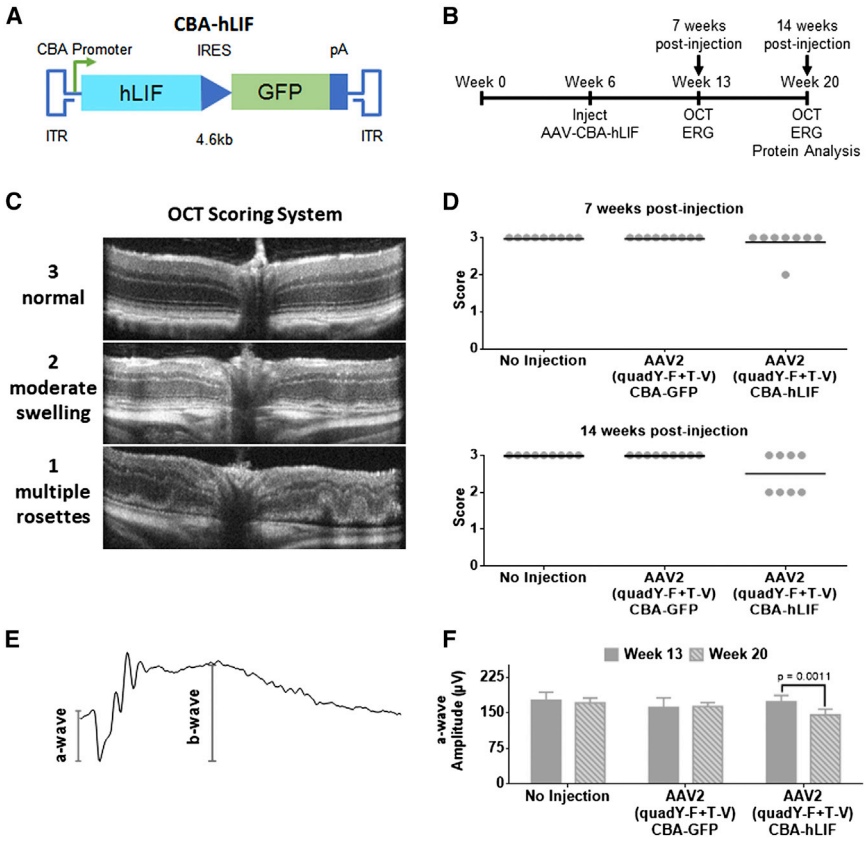

Figure 1. Long-Term, Constitutive Expression of AAV-hLIF Leads Can Have Adverse Effects on Retinal Morphology and Function

(A) Schematic of AAV-hLIF construct showing the human LIF (hLIF) transgene under the control of the chicken beta actin (CBA) promoter. The expression construct is flanked by inverted terminal repeats (ITRs) to allow for packaging into AAV vectors. The size of the vector is 4.6 kb. (B) Experimental timeline using the AAV-hLIF vector. At 6 weeks of age, BALB/cJ mice were intravitreally injected with AAV2 (quadY-F+T-V) carrying the hLIF transgene. *In vivo* imaging and functional analysis was performed 7 weeks and 14 weeks post-injection. (C) Scoring rubric for assessment of retinal morphology. A score of 3 indicated a normal retina that maintains well-defined boundaries of hyper- or hypo-reflectance. A score of 2 indicated retinas with minor ruffling and less-defined retinal layer boundaries. Retinas with a score of 1 had multiple rosettes, retinal thinning, excessive cells in the vitreous, and retinal detachment. (D) Retinal scoring in low titer control and AAV2 (quadY-F+T-V) hLIF-injected animals 7 (top) and 14 (bottom) weeks post-injection. Each filled circle represents one animal (n = 8–9), and the black lines represent the mean for each group. (E) Representative ERG trace. The a-wave, the initial negative deflection, reflects the hyperpolarization of the photoreceptors following light stimulation. The b-wave amplitude was measured from the trough of the a-wave to the adjacent peak, indicative of the depolarization due to voltage changes taking place in the inner retina. (F) Average a-wave amplitudes at 1.0 cd.s/m^2 of control injected and AAV2 (quadY-F+T-V) hLIF-injected animals 7 and 14 weeks post-injection. Error bars represent SEM for each group. One-way ANOVA with Sidak post-hoc test was performed; n = 8 animals per group.

RESULTS

Unregulated, Long-Term Cytokine Expression Is Detrimental to the Retina

In this study, we utilized an AAV2 mutant capsid to deliver the human LIF (hLIF) transgene to the retina by intravitreal injection. This capsid contains four proteasomal avoidance mutations and is referred to as AAV2 (quadY-F+T-V). AAV2 (quadY-F+T-V) was selected since it can efficiently transduce a broad range of cell types in the murine retina by intravitreal injection (Figure S1A).[38] Additionally, the AAV2 capsid is the only AAV serotype that can effectively transduce retinal cells in non-human primates.[39]

An AAV2 (quadY-F+T-V) vector expressing the hLIF transgene under the control of the chicken beta-actin (CBA) promoter was injected into the vitreous of BALB/cJ mice at two titers (1×10^8 vector genomes/μL for low titer, 1×10^9 vector genomes/μL for high titer) (Figure 1A). GFP expression from this vector was not detectable by native fluorescence or immunohistochemistry (IHC) with antibodies to GFP. After 7 weeks, using a well-established light damage (LD) model, mice were exposed to damaging bright light that was calibrated to synchronously kill the majority of photoreceptors. Mice injected with AAV2 (quadY-F+T-V)-hLIF had significant preservation of photoreceptors in the outer nuclear layer (ONL) compared to AAV2 CBA-GFP controls (Figure S2). However, despite this protective activity, long-term studies on treated mice not exposed to damaging light had progressive, abnormal retinal structures consistent with edema, as seen by optical coherence tomography (OCT) imaging (Figures 1B–1D). Long-term expression also caused a reduction in photoreceptor light responses, as measured by electroretinography (ERG) (Figures 1E and 1F). We observed edema in animals treated with the low titer of AAV2 (quadY-F+T-V)-hLIF, which was significantly worse in the high-titer group (Figure S3A). The severity of adverse retinal changes (edema and loss of function) correlated with the level of LIF protein expression and activation of STAT3 (Figures S3B and S3C). Overall, these results demonstrate that unregulated, high levels of LIF expression would be of limited therapeutic value.

Development of RFP2

In our initial attempt to regulate LIF expression, a synthetic and codon-optimized *E. coli* DHFR (DD) cDNA was fused to the hLIF cDNA (Figure S4A). While the resulting fusion protein was expressed in cell culture, it was not regulated by TMP and was unable to activate STAT3 downstream of its receptor (Figures S4B and S4C). Our

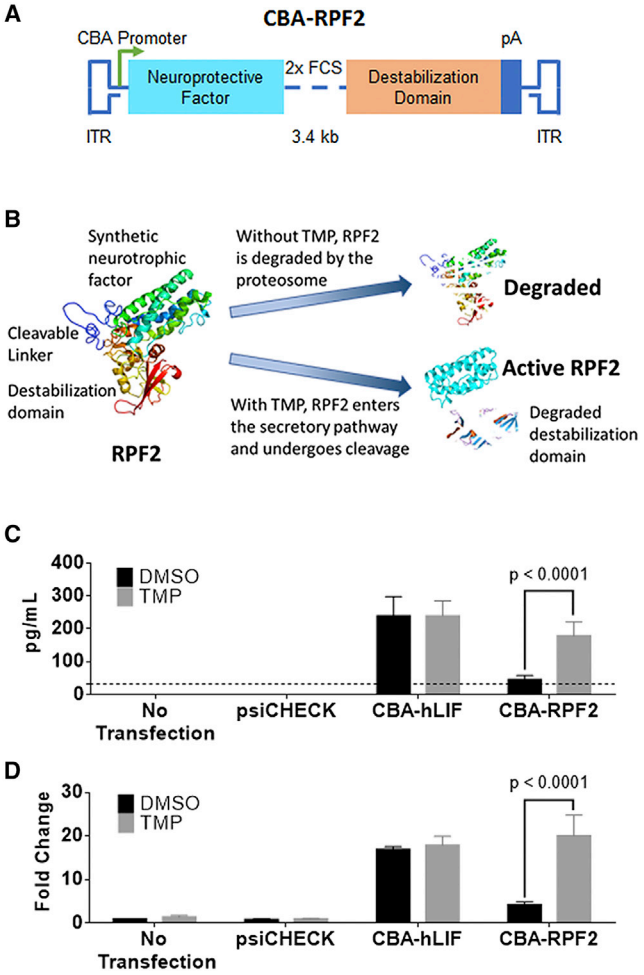

Figure 2. TMP-Stabilized RPF2 Is Active *In Vitro*

(A) Schematic of the RPF2 construct showing the synthetic neuroprotective factor linked to the destabilization domain expressed from the CBA promoter. Within the linker region, two FURIN cleavage sites (FCS) separate the domains. (B) Illustration of the RPF2 stabilization strategy. In the absence of TMP, RPF2 is rapidly degraded by the proteasome following translation. TMP stabilizes RPF2, allowing it to be processed and secreted. (C) ELISA measuring cytokine levels in the media of rMC-1 cells transfected with CBA-RPF2 with or without TMP. Dotted line indicates the limit of detection of the ELISA assay at 32 pg/mL. (D) Immunoblot analysis of pSTAT3 Y705 levels in rMC-1 cells following treatment with conditioned media from CBA-RPF2-transfected cells, with and without TMP treatment. Error bars represent SEM (C and D). Two-way ANOVA with Sidak post-hoc test was performed for (C) and (D); n = 4 biological replicates.

interpretation of these results was that both domains in the fusion protein inhibited the activity of the other. In attempts to produce a regulatable and functional cytokine, we added either (1) sequences encoding an 8-amino-acid linker with one FURIN cleavage site (FCS) between hLIF and the DD or (2) sequences encoding a 12-amino-acid linker with 2× FCS (Figures 2A and S4A). This strategy takes advantage of the FURIN protease system that cleaves the domains as they transit the secretory pathway.[40] The fusion proteins were tested *in vitro*, and the 12-amino-acid linker containing 2× FCS produced the highest levels of cleaved cytokine with TMP treatment and had minimally detectable levels of cytokine in the absence of TMP (Figures 2B and 2C). In addition, the expression of cleaved and secreted cytokine was regulated by TMP in a dose-dependent manner (Figure S4D). The effects of TMP were dependent on the DD fusion, since TMP did not alter the expression of cytokine in the luciferase-expressing control plasmid (psiCHECK) or hLIF-transfected groups. To determine whether the secreted RPF2 was functional, the conditioned media from transfected cells were collected and used to stimulate STAT3 in untransfected rat Müller glial-like (rMC-1) cells. Only conditioned media from TMP-treated cells led to a significant increase in STAT3 activation (Figure 2D). These levels were comparable to that of the hLIF-transduced group. Our *in vitro* data suggest that RPF2 can be regulated in a dose-dependent manner and can be secreted in its functional form to activate STAT3. Because of its superior regulation, the fusion protein with 2× FCS, named RPF2, was packaged into AAV for further testing.

AAV-RPF2 Is Regulated by TMP in a Dose-Dependent Manner *In Vivo*

RPF2 was packaged into the AAV2 (quadY-F+T-V) capsid and intravitreally injected into BALB/cJ mice at high and low titers. Six weeks after AAV injections, mice were given 7 daily intraperitoneal (i.p.) injections of varying doses of TMP. RPF2 levels rose with increasing doses of TMP, reaching a maximum fold change of 6.19 and falling to baseline following a 7-day TMP withdrawal (Figures 3A and S5A). Cytokine levels for both the TMP-vehicle only (0 mg/kg) and TMP withdrawal groups were below the limit of detection for the assay. The expressed cytokine was also functional, since STAT3 activation in the retina was higher in animals treated with TMP (Figure S5B). To characterize the long-term effects of the AAV-mediated RPF2 expression, retinal structure and function were monitored over time following intravitreal injection (Figure 3B). Animals were placed on chow containing TMP starting at 7 weeks post-injection. This route of drug administration yielded RPF2 stabilization at levels comparable to that of the 60 mg/kg systemic TMP delivery and did not affect the animal's daily food intake (Figures S5C and S6). After 7 weeks of TMP treatment, mice injected with AAV2 (quadY-F+T-V)-RPF2 had normal retinal morphology and clearly lacked the edema observed in the AAV2 (quadY-F+T-V)-hLIF-treated mice (Figures 1D, 3C, and S5D). Mice also had normal photoreceptor function, as reflected in scotopic ERG responses (Figure 3D). These data show that AAV-mediated RPF2 expression can be regulated by TMP in a dose-dependent manner *in vivo*, and long-term expression does not result in the negative outcomes that we observed using AAV2 (quadY-F+T-V)-hLIF.

AAV-RPF2 Can Protect Photoreceptors from Acute Light Injury

To determine whether an AAV-mediated RPF2 therapy could protect photoreceptors from LD, 6-week-old BALB/cJ mice were injected with AAV2 (quadY-F+T-V)-RPF2 at low and high titers. After 7 weeks, mice were given TMP in mouse chow for 7 days prior to exposure to damaging bright light (Figure 4A). In the presence of

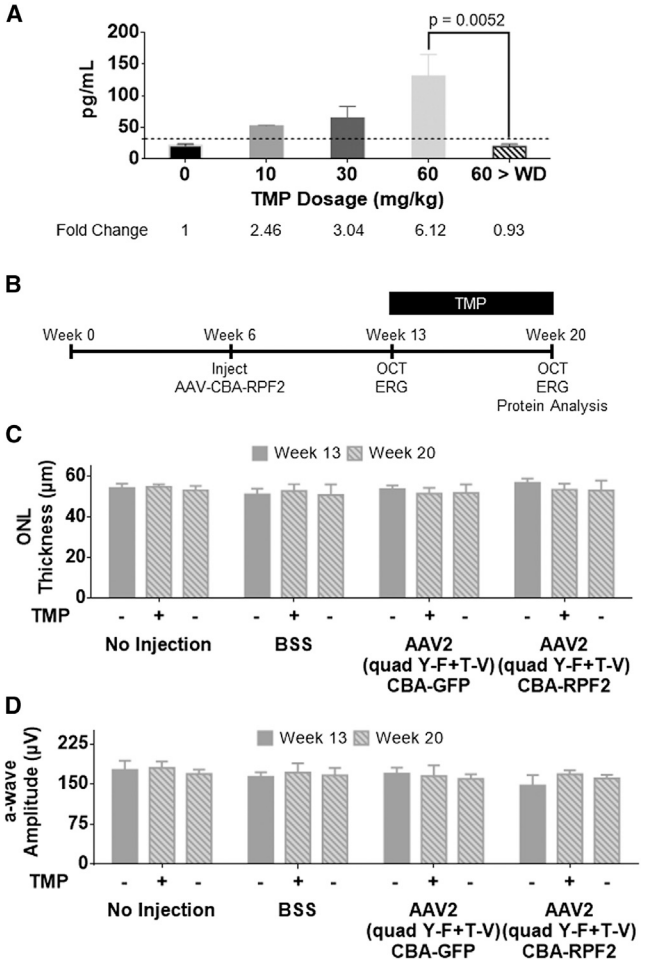

Figure 3. RPF2 Is Regulated in a Dose-Dependent Manner and Demonstrates No Toxicity *In Vivo*

(A) ELISA levels of RPF2 in the retinal lysates of animals injected with low-titer AAV2 (quadY-F+T-V) RPF2 at varying concentrations of TMP. Tissue was also collected 7 days after TMP withdrawal (60 > WD). Dotted line indicates the limit of detection of the ELISA assay at 32 pg/mL. One-way ANOVA with Sidak post-hoc test was performed; n = 4 biological replicates. (B) Experimental timeline using the AAV2 (quadY-F+T-V) RPF2 vectors following a similar strategy to that in Figure 1B. From week 13 to week 20, mice were kept on either normal chow or a TMP-supplemented diet. (C) Average outer nuclear layer (ONL) thickness in injected animals before and after TMP diet. (D) Average a-wave amplitudes at 1.0 cd.s/m^2 of control-injected and AAV2 (quadY-F+T-V) RPF2-injected animals 7 and 14 weeks post-injection. Two-way ANOVA with Sidak post-hoc test was performed for (C) and (D); n = 8 biological replicates. No statistical significance was found. BSS, balanced saline solution. Error bars represent SEM.

TMP, animals injected with AAV2 (quadY-F+T-V)-RPF2 showed significant preservation of ONL thickness compared to control-injected or no-TMP control groups, suggesting that the TMP-induced cytokine protected photoreceptors (Figure 4B). TMP-induced RPF2 not only preserved structure, but also preserved photoreceptor function (Figure 4C). High-titer AAV-RPF2 groups had greater preservation of the ONL than the low-titer groups (Figures S7A–S7C).

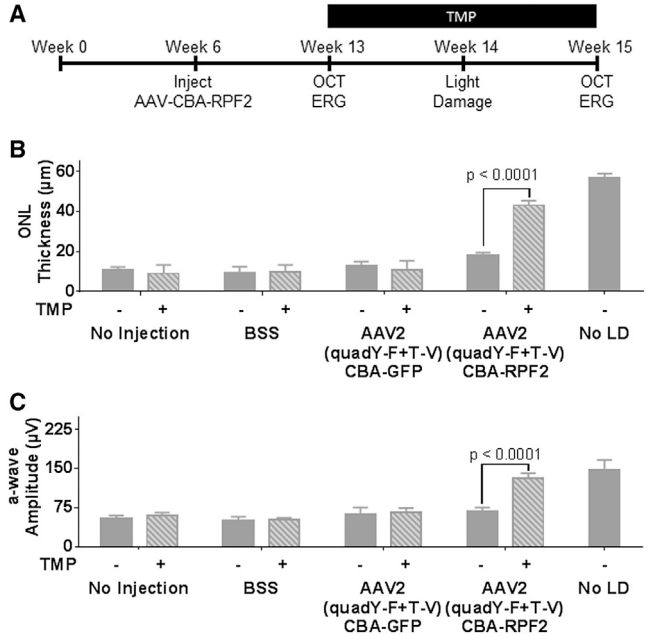

Figure 4. RPF2 Can Reduce Retinal Degeneration in an Acute Light Damage Model

(A) Experimental timeline using the AAV2 (quadY-F+T-V) RPF2 vectors with light damage (LD). One week after the start of TMP supplementation, animals were LD treated, followed by a week of recovery to allow of clearance of damaged cells. (B) Average ONL thickness in injected animals after LD treatment. (C) Average a-wave amplitudes at 1.0 cd.s/m^2 of control and AAV-RPF2-injected animals after LD treatment. Error bars indicate SEM for (B) and (C). Two-way ANOVA with Sidak post-hoc test was performed for (B) and (C); n = 8–9 biological replicates per group.

Overall, the AAV-RPF2 therapy successfully protected the murine retinas from acute light injury.

AAV-RPF2 Protects Photoreceptors in a Model of Inherited Retinal Degeneration

The *rd10* mouse is a widely used model to study inherited retinal degeneration.[41–45] To determine whether TMP-induced RPF2 expression could preserve photoreceptors in *rd10* retinas, AAV2 (quadY-F+T-V)-RPF2 was intravitreally injected at high titer to the animals at 2 weeks of age, prior to any degeneration (Figure 5A). At week 3 (weaning age), mice were provided TMP chow, and the animals were monitored by OCT and ERG over time. The TMP-treated AAV-RPF2 groups had significant preservation of the ONL compared to no TMP controls (Figure 5B). Retinas were collected at week 8 to measure preservation of cones, which normally die subsequent to rod loss. In the AAV-RPF2 groups treated with TMP, cones were markedly preserved compared to control-injected mice or no-TMP controls (Figures 5C and 5D). The preserved cones maintained majority of their function in the TMP-treated AAV-RPF2 groups, as measured by photopic ERG responses (Figure 6A). To quantify functional vision in treated mice, we used OptoMotry to measure optokinetic reflex (Figure 6B).[46,47] The AAV2 (quadY-F+T-V)-RPF2 group treated with TMP showed significant

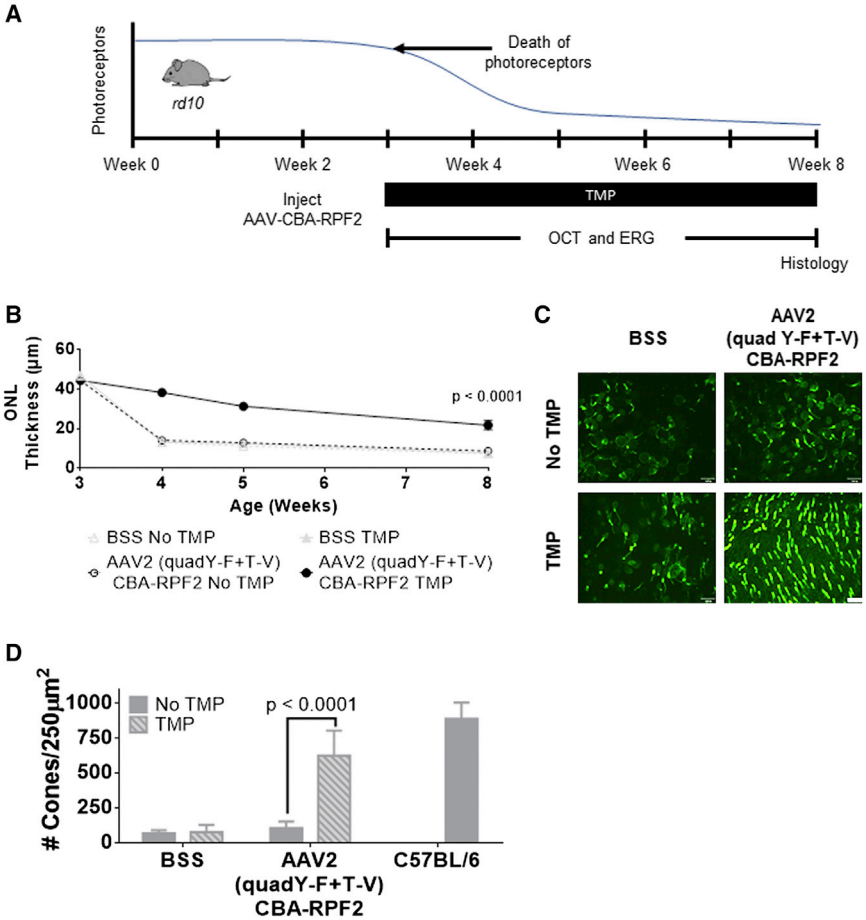

Figure 5. RPF2 Can Preserve Cone Morphology in the Inherited *rd10* Retinal Degeneration Model

(A) Timeline showing the natural history of the *rd10* mouse model and therapeutic intervention with AAV2 (quadY-F+T-V) RPF2 vectors. The onset of photoreceptor degeneration begins at week 3. Animals were injected with AAV2 (quadY-F+T-V) RPF2 vectors at 2 weeks of age. At weaning, animals were placed on a TMP diet. Morphological and functional analysis was performed over the subsequent weeks before collecting the eyes for histology. (B) Average ONL thickness in therapy-treated animals over time. Two-way ANOVA with Sidak post-hoc test was performed; n = 6 biological replicates per group. Error bars indicate SEM. (C) Immunofluorescent images of retinal flat mounts showing staining of s and m opsin (green). Images were taken at 40× magnification. White bar indicates 100 µm. (D) Quantification of cones in (C). Error bars indicate SEM. Two-way ANOVA with Sidak post-hoc test was performed; n = 4 biological replicates per group, except C57BL/6 = 3 biological replicates. BSS, balanced saline solution.

preservation of cone-mediated visual behavior compared to control-injected or no-TMP groups. Responses in TMP-treated mice were comparable to that of C57BL/6J wild-type control mice (Figure 6C). Overall, our data show AAV-mediated RPF2 expression is capable of protecting both rods and cones and preserving cone vision in this aggressive model of inherited retinal degeneration.

DISCUSSION

In this study, we tested RPF2 in two different models of degeneration to determine its ability to protect from a broad spectrum of insults. The LD model is a well-established method to synchronously induce photoreceptor death.[29] Cellular damage is believed to be caused by the formation of free radicals, resulting in cell loss.[48] In diseases like AMD, where oxidative stress is believed to be a contributing factor in disease progression, administration of RPF2 could be beneficial. For our second model, we used a mouse with an inherited mutation in the beta subunit of rod phosphodiesterase, a critical component of the phototransduction pathway. This mutation leads to aggressive retinal degeneration, with extensive retinal remodeling within the first month of life. For the maintenance of useful vision in humans, it is of paramount importance to keep cones functional, since humans predominantly utilize cones in their central vision. We showed that AAV-mediated RPF2 expression preserves both rods and cones and promotes maintenance of useful vision.

A major advancement in gene therapy has been the development of regulated transgene expression. These systems involve the use of exogenous effector molecules like tetracycline, rapamycin, Shield-1, or TMP to control transcription, dimerization, and post-translational stability.[33,49–54] Transcriptional regulation has been mediated by using tetracycline-regulated bacterial transcription factors and their target promoters. A benefit of using tetracycline promoters is that they have a wide dynamic range of induced gene expression and are reversible. However, this system is a dual-transgene approach that may have limited utility from a single AAV gene delivery. In addition, this system has been shown to induce unwanted immune responses in non-human primates and can suffer from leaky or ectopic transgene expression.[55–57] A dual-AAV vector approach using rapamycin-induced dimerization has also been developed.[52,58] This system requires the expression of fusion proteins with the FK506 binding protein (FKBP)-rapamycin binding domain that are only dimerized in the presence of rapamycin. This system works primarily intracellularly and typically involves the transduction of two distinct AAV vectors into the same cell. A drawback of this design is that the dual vector approach is less efficient than utilizing a single vector.[59] A second disadvantage is in the use of rapamycin, which has biological activity independent of the transgene.[60] Moreover, this system is not well-designed to directly regulate secreted proteins. Autoregulatory promoters are an alternative to the exogenous effectors.[61,62] However, these cannot be controlled at will, and if the promoters do not express at high levels, they are at risk of being silenced over time.[63]

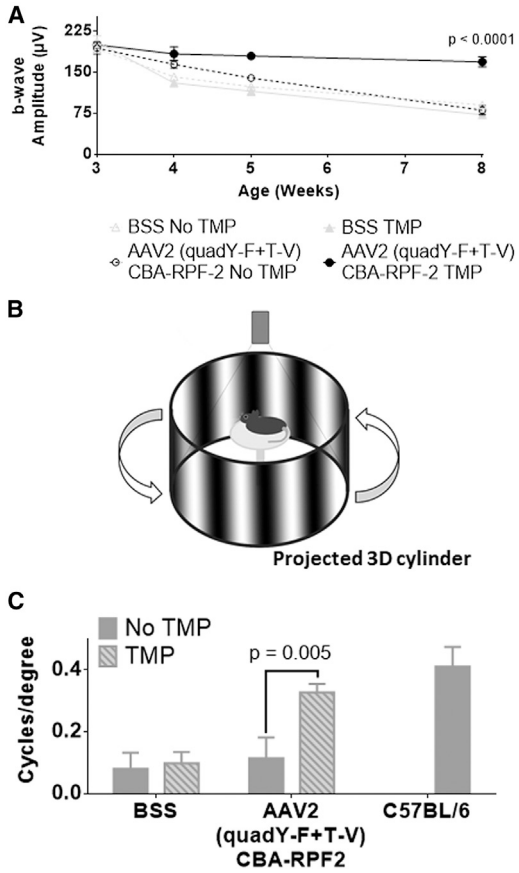

Figure 6. RPF2-Treated *rd10* Mice Maintain Long-Term, Cone-Dependent Vision

(A) Average b-wave amplitudes at photopic 60 cd.s/m^2 of control and AAV2 (quadY-F+T-V) RPF2-injected animals over time. (B) Illustration of the OptoMotry system used to measure optokinetic-tracking response in therapy-treated animals. Animals stand on an elevated platform surrounded by computer monitors that display a sine wave grating, creating a virtual cylinder. The animals track the rotation of the cylinder with reflexive head and neck movements, which is detected by an overhead camera. (C) Quantification of optokinetic responses from the OptoMotry analysis described in (B). Error bars indicate SEM for (A) and (C). Two-way ANOVA with Sidak post-hoc test was performed for (A) and (C). For (A), n = 6 biological replicates per group. For (C), n = 4 biological replicates per group, except C57BL/6 = 2 biological replicates. BSS, balanced saline solution.

Additionally, autoregulatory systems are not tunable to meet the personalized needs of the patient and are not reversible. Post-transcriptional control using microRNAs have the same limitations and may have significant off-target effects.[64]

Related to the work in this study, multiple DDs have been developed to regulate the stability of transgene expression.[33,54,65,66] The first of these was the FKBP-Shield-1 system, which used a mutated FKBP domain that was unstable in the absence of the chemical chaperone Shield-1.[54] Following a similar strategy, the DHFR-TMP system used in this study was developed.[33] The advantages of using chaperone-regulated DDs are their ability to be rapid and tightly regulated over a broad dynamic range by adjusting dosing of the chaperone and transgene expression can be easily reversed if needed by drug withdrawal.[33,54] Both systems have compact coding regions and can be delivered in a single AAV vector. An advantage of the DHFR-TMP system is that TMP is an FDA-approved, orally available drug that can cross the blood-brain barrier.[67] TMP is commonly used as an ophthalmic drug to treat bacterial infections, thus proving the drug is safe and effective in the eye.[68] These features greatly reduce the barrier for therapeutic use in humans. Current studies have shown that there are no immunogenic properties associated with the DHFR DD.[34] Combining this approach with a high-expressing promoter, we can reduce the potential silencing effects seen in low-expressing promoters. Overall, this makes the DHFR-TMP system attractive for use in the central nervous system.

To determine appropriate TMP dosing to use in mice, we used a well-established, allometric approach for scaling the mouse dose based on the human equivalent dose (HED), which is described in the Materials and Methods.[69,70] The TMP dose range used in this study (20–60 mg/kg) was equivalent to 1.6–4.9 mg/kg HED, which is in the lower range of the recommended dosage for humans (6–20 mg/kg).[71] Since TMP is an antibiotic, there might be concerns that chronic administration of the drug could alter the microbiota of the gut, adversely affecting the patient. Our animals on the TMP diet did not show any difference in feeding or behavior when compared to the control animals placed on normal chow (Figure S6). Additionally, control animals fed with TMP had no changes to retinal function or morphology (Figure 3). Studies on the long-term use of TMP in patients with pneumocystis pneumonia, urinary tract infections, and acute lymphoblastic leukemia all found TMP to be safe with multiple years of continuous therapy, with minimal adverse effects.[72–74] Moreover, to avoid systemic delivery, TMP has been formulated for delivery as topical eye drop for localized administration.[68] Withdrawal of TMP reduced RPF2 levels to baseline, which further demonstrates the tightly controlled regulation of this system. This is appealing when applying our therapy to a clinical setting because in the event of adverse effects, the therapy has the ability to be stopped quickly.

Recently, the gene-therapy field has achieved significant breakthroughs, including the FDA approval of the cell-based gene therapy known as Kymriah to treat precursor B cell lymphoblastic leukemia.[75] In addition, the first gene replacement therapy was granted FDA approval for treatment of an inherited retinal disorder.[76] This is especially significant, since it utilizes the AAV platform to deliver a normal copy of the *RPE65* gene to patients with Leber's congenital amaurosis, who have a mutation in this gene. The success of this therapy opens doors for developing gene-based treatments for a variety of other retinal disorders. Our results suggest that broad-spectrum protection could be provided by RPF2 as a primary, standalone treatment to prevent retinal degeneration. Alternatively, it could be used as an adjunct to a gene-replacement therapy. For example, in patients given AAV-*RPE65*, there was successful gene replacement and rescue of function, but cell loss persisted over time.[77,78] AAV-RPF2 could

potentially be used to expand the therapeutic window for patients with inherited retinal disorders, keeping the cells alive long enough for secondary intervention.[79] In addition, stem cells poorly survive in a degenerating environment.[80] Long-term studies have shown that after integration, stem cells die over time, so a combinatorial approach using AAV-RPF2 could improve the efficacy of this treatment.[81] Overall, this work is a promising step toward improved, broad-spectrum treatment options for patients suffering from retinal disease.

MATERIALS AND METHODS

Mice

All procedures were performed according to the Association for Research in Vision and Ophthalmology Statement for the Use of Animals in Ophthalmic and Vision Research and in compliance with protocols approved by the University of Florida. BALB/cJ, C57BL/6, and *rd10* breeders were obtained from The Jackson Laboratory (Bar Harbor, ME). Colonies were established at the internal rodent breeding program at the University of Florida. All mice were reared in 12-hr cyclic dim light (<100 lux)/dark conditions (6:00 a.m.-6:00 p.m.) in the University of Florida animal housing facility and provided water and food *ad libitum*.

AAV Vector Construction and Virus Production

The AAV vector plasmid pTR-UF11 contains the full chimeric CBA driving GFP cDNA.[82] The AAV vector plasmid pTR-CBA-hLIF contains the CBA promoter driving hLIF cDNA followed by an internal ribosome entry site and a GFP cDNA. The internal ribosome entry site (IRES) was considered to be non-functional since no GFP expression was detected *in vivo* and *in vitro*. This plasmid was generously provided by Dr. Sergei Zolotukhin.[83] The AAV vector plasmid pTR-CBA-RPF2 contains the CBA promoter driving the RPF2 cDNA. The RPF2 cDNA was created by *de novo* synthesis from Genscript (Piscataway, NJ). The rep-cap plasmid containing AAV2 cap with Y272F, Y444F, Y500F, Y730F, and T491V mutations has been previously described.[38] The vector plasmid, AAV rep-cap, and Ad helper plasmid were co-transfected into HEK293T cells, and the viruses were harvested and purified as previously described.[84] Purified viruses were resuspended in balanced salt solution (BSS) (Alcon, Ft. Worth TX), supplemented with Tween 20 (0.014%), and stored at −80°C until use. All viruses were titered by qPCR and tested for endotoxin.

Cell Culture Transfections, TMP Treatment, and Conditioned Media Experiments

The rMC-1 cell line was generously provided by Dr. Vijay Sarthy.[85] The cells were cultured in high-glucose DMEM supplemented with 10% fetal bovine serum, 100 U/mL penicillin, 100 μg/mL streptomycin, and 1× GlutaMax (Thermo Fisher Scientific, Waltham, MA). At 80% confluency, the cells were transfected with a purified plasmid (Table S1) using the standard Lipofectamine 3000 protocol (Thermo Fisher Scientific, Waltham, MA). 24 hours after transfection, the media was replaced with serum-free DMEM. The cells were dosed overnight with varying concentrations of TMP or control vehicle (20% DMSO). The conditioned media was then collected for ELISA or STAT3 activation studies. For conditioned media experiments, rMC-1 cells were grown in 6-well plates. The serum-deprived cells were incubated for 30 min with conditioned media collected from transfected rMC-1 cells treated with TMP. The cells were then washed with cold PBS and harvested for analysis by immunoblotting.

Immunoblotting

Retinal tissue or rMC-1 cells were homogenized in radioimmunoprecipitation assay (RIPA) buffer (Sigma-Aldrich, St. Louis, MO) containing a protease inhibitor cocktail (Merck Millipore, Billerica, MA) supplemented with sodium fluoride and sodium orthovanadate (New England Biolabs, Ipswich, MA). Protein lysate concentration was quantified by BCA assay (Thermo Fisher Scientific, Waltham, MA) before boiling and subjecting to SDS-PAGE. Lysates were run on 4%–20% polyacrylamide gel (Thermo Fisher Scientific, Waltham, MA) and transferred onto polyvinylidene fluoride membranes (Merck Millipore, Billerica, MA). Membranes were blocked with Odyssey blocking buffer (LI-COR Biosciences, Lincoln, NE) and incubated overnight with primary antibodies (Table S2). Secondary antibodies conjugated with IRDyes (Table S2) were used. Signals were detected using the Odyssey CLx Imaging System (LI-COR Biosciences, Lincoln, NE). Intensities of the protein bands were quantified using Image Studio 5 (LI-COR Biosciences, Lincoln, NE).

ELISA

LIF and RPF2 levels were detected in retinal tissue lysates and rMC-1 conditioned media. For tissue lysates, the retinas were prepared in an ELISA lysis buffer (1% octylphenoxypolyethoxyethanol-CA-630 [IGEPAL-CA 630], 135 mM NaCl, 20 mM Tris, and 2 mM EDTA). Lysates or conditioned media were incubated for 2 hr on plates containing pre-blocked capture antibodies followed by 1 hr incubations with biotinylated detection antibody and streptavidin conjugated to horseradish peroxidase (Table S2). Signals were developed using the Substrate Reagent Pack (R&D Systems, Minneapolis, MN) and read at a 450-nm wavelength using the CLARIOstar microplate reader (BMG LABTECH, Ortenberg, Germany).

TMP Delivery

For the *in vivo* dose response, varying concentrations of TMP were resuspended in a solution of 20% DMSO. The mice were i.p. injected once per day for 7 days with equal volumes of the varying TMP dosage or vehicle. For the reversal study, mice were injected once per day for 7 days followed by no administration of the drug for a subsequent 7 days before the retinas were harvested for ELISA analysis. For the TMP food supplement, 600 ppm of TMP was added to the Teklad LM-485 mouse diet (Envigo, Huntingdon, United Kingdom). The TMP chow was provided *ad libitum* to the mice. To calculate the TMP HED, a well-established, allometric approach that considers the body surface area and not just the individual's weight can be used. The formula is as follows: HED = Mouse dose (mg/kg) * (mouse Km/human Km). Km represents the body surface area to mass ratio, and the values for each species can be found in Table 1 of Regan-Shaw et al.[69] The human Km for a 60-kg individual

is 37, and the mouse Km for a 20-g mouse is 3. The minimum dose used in this mouse study was 20 mg/kg: 20 * (3/37) = 1.62 mg/kg HED. The maximum dose used in this mouse study was 60 mg/kg: 60 * (3/37) = 4.86 mg/kg HED.

Intravitreal Injections

Mice were anesthetized with ketamine (70–100 mg/kg) and xylazine (5–10 mg/kg). The eyes were dilated with a single drop of tropicamide and phenylephrine (Alcon, Ft. Worth TX). 1 μL of viral vector or BSS (Alcon, Ft. Worth TX) were separately injected into the vitreous through the temporal limbus of the eye using a syringe with a 33G needle (Hamilton Company, Reno, NV). AK-Poly-Bac ophthalmic medication (Alcon, Ft. Worth TX) was used to prevent post-surgical infections and suppress inflammation. Eyes were evaluated by OCT 1 week post-injection, and any animals with unresolved surgical trauma were excluded from the study.

ERG

Mice were anesthetized with ketamine (70–100 mg/kg) and xylazine (5–10 mg/kg). The eyes were dilated with a single drop of tropicamide and phenylephrine (Alcon, Ft. Worth TX). Retinal function was measured using the Colordome ERG system (Diagnosys, Dorset, UK). To record electrical responses from both eyes, gold wire electrodes were placed on the corneas, a platinum reference electrode was placed in the mouth, and a platinum ground electrode was attached to the tail. The body temperature was maintained at 37°C throughout the experiment using the built-in heating pad of the ERG system. For scotopic ERGs, the animals were dark-adapted for at least 12 hr. A series of increasing light flash intensities ranging from 0.0001–180 cd.s/m^2 was used. The a-wave was defined as the trough of the negative deflection from the baseline, while the b-wave was measured from the a-wave to the peak of the positive deflection. For photopic ERGs to measure cone function, a background illumination of 30 cd.s/m^2 was used to block rod photoreceptor contribution to the recording. A series of increasing light flash intensities above the background illumination (photopic 1.875–60 cd.s/m^2) were used to generate a cone response. Established photopic protocols solely measure the b-wave, since cone photoreceptors make up only a minor population of retinal cells, resulting in a-wave values near the noise levels for most ERG setups.

Spectral Domain-OCT and Scoring

For *in vivo* retinal imaging, Spectral Domain-OCT images were obtained using the Envisu C-Class OCT system (Leica Microsystems, Wetzlar, Germany). Mice were first anesthetized with ketamine (70–100 mg/kg) and xylazine (5–10 mg/kg), followed by dilation with a single drop of tropicamide and phenylephrine (Alcon, Ft. Worth, TX). Cornea clarity was maintained using GenTeal lubricating eye gel (Novartis Pharmaceuticals, Basel, Switzerland). The mice were placed on a custom-built stage secured with a bite bar to allow free rotation for imaging. The stage was adjusted manually to center the image of the retina at the optic nerve head. Cross-sectional images were generated using 425 rectangular volume scans, which were averaged every five scans prior to image analysis. Images were acquired for both eyes. Averaged OCT images were analyzed using InVivoVue 2.4 (Leica Microsystems, Wetzlar, Germany). ONL thickness was measured using the linear caliper function in the software by a masked observer using a pre-established uniform grid (Figure S2, top panel). The OCT images were also graded by a masked observer utilizing a scoring system ranging from 1 to 3 (Figure 1C). A score of 3 indicated a healthy and normal retina with no thinning and little to no inflammation. A scoring of 2 indicated a retina with slight edema, minor thinning, or inflammation. A scoring of 1 signified a degenerated retina with severe thinning, severe inflammation, missing external limiting membrane, or visible retinal detachment.

IHC

To obtain retinal tissue sections, mouse eyes were enucleated with forceps and placed in cold PBS. Under a dissecting microscope, the cornea and lens were dissected away and the remaining eye cup was processed for cryosectioning. With additional eyes, retinal flat-mounts were prepared by gently dissecting the retina from the eyecup. Four incisions were made from the periphery to the center of the retina to flatten the retina onto a microscope slide. Eyecups and flat mounts were fixed in 4% paraformaldehyde for 30 min at room temperature. The fixed eyecups were cryopreserved in 30% sucrose in PBS overnight at 4°C. The samples were embedded in Tissue-Tek OCT Compound (Sakura Fintek USA, Torrance, CA) and immediately frozen in liquid nitrogen. Tissue sections were cut at a thickness of 16 μm on a cryostat and placed onto glass slides. Slides were stored at −20°C until needed for immunostaining. For IHC, the flat-mount retinas or eyecup sectioned slides were washed with PBS containing 1% Triton X-100 (PBS-T). To prevent non-specific binding, the tissue was blocked with 10% horse serum in PBS-T for at least 1 hr at room temperature. Primary antibody (Table S2) was applied to each sample for incubation overnight at 4°C. Samples were washed with PBS-T before incubating with secondary antibody (Table S2) for 1 hr at room temperature. Nuclei were counterstained with DAPI before mounting with glass coverslips using 60% glycerol. Imaging was performed using the BZ-9000 fluorescence microscope (Keyence, Osaka, Japan). The exposure time of each fluorescent channel was kept constant between samples for a given antibody. For flat-mount counting of cone outer segments, a 250-$μm^2$ grid was superimposed over five random areas of each flat mount image. Cells that were positive for the cone opsin staining were counted within the grid and averaged. All data quantification was completed by a masked observer.

LD

For light damage (LD) experiments, two mice were placed in a cage with a modified lid equipped with LED lights (white light). Prior to damage, the light intensity was measured using a light meter (Thermo Fisher Scientific, Waltham, MA) and set to 1,200 lux using the connected dimmer. The mice were exposed to the damaging light for 4 hr (6:00 p.m.–10:00 p.m.). Once the experiment ended, the mice were moved back into dim lighting conditions to recover for 1 week before downstream analysis was performed. The lighting equipment was available at the UF animal facility and was approved

by the ACS. All mice were kept in a ventilated rack for the duration of the experiment.

OptoMotry

To test the optokinetic reflex of mice, we used the OptoMotry system developed by CerebralMechanics (Lethbridge, Canada). This system consisted of four computer screens that display alternating vertical light and dark bars that appear as a virtual, rotating, 3D cylinder. The mouse was placed on a non-rotating pedestal in the middle of the enclosure. The 3D cylinder pattern was rotated at a fixed speed of 12 deg/s, and the contrast was maintained at 100%. Head tracking was monitored using an overhead camera, which was recorded by a masked observer. The staircase method was used to determine visual acuity by establishing the threshold of spatial frequency that the animal can track. An animal was considered to be tracking if its head followed the direction of the stimulus with a speed similar to the pattern movement.

Fundus Imaging

For fundus imaging, a Micron III camera (Phoenix Research Labs, Pleasanton, CA) was used. Mice were anesthetized with ketamine (70–100 mg/kg) and xylazine (5–10 mg/kg) and dilated with a single drop of tropicamide and phenylephrine (Alcon, Ft. Worth, TX). Corneal clarity was maintained using GenTeal lubricating eye gel (Novartis Pharmaceuticals, Basel, Switzerland). The mice were stabilized on a custom holder that allowed adjustments to center the image of the retina at the optic nerve head. Imaging was performed under bright-field illumination and using filtered red and green channels. Images were acquired for both eyes.

Statistical Analysis

Statistical analysis was carried out using Prism 6 (GraphPad Software, La Jolla, CA). Statistical significance between multiple groups was determined by using ANOVA.

SUPPLEMENTAL INFORMATION

Supplemental Information includes seven figures and two tables and can be found with this article online at https://doi.org/10.1016/j.ymthe.2018.07.016.

AUTHOR CONTRIBUTIONS

C.P.S. and J.D.A. conceived RPF2 and designed the experiments. C.P.S., C.J.K., and A.A.I. performed experiments. C.P.S., C.J.K., and J.D.A. prepared the manuscript. S.L.B. contributed advice on AAV serotype and S.L.B. and S.E.B. provided feedback on the manuscript. J.D.A. acquired funding.

CONFLICTS OF INTEREST

The authors declare no competing financial interests.

ACKNOWLEDGMENTS

We would like to thank Dr. William Hauswirth and the University of Florida's Ocular Gene Therapy Core for manufacturing the AAV vectors, Dr. Sergei Zolotukhin for the pTR-CBA-hLIF vector, and Dr. Vijay Sarthy for providing the rMC-1 cell line used in this study. We also thank Dr. Wesley Clay Smith, Dr. Jorg Bungert, Dr. Alfred Lewin, Dr. Christhian Idelfonso, Dr. Shreyasi Choudhury, Dr. Seok Hong Min, Raghav Pai, Eric Nayman, Lei Xu, Marcus Hooper, Emily Brown, Michael Massengill, and Meagan Ash for their assistance on this project. This work was supported by the Foundation for Fighting Blindness, the National Eye Institute (grant #R01EY016459), and an unrestricted departmental grant from the Research to Prevent Blindness. This work was performed at the University of Florida in Gainesville, FL.

REFERENCES

1. Veleri, S., Lazar, C.H., Chang, B., Sieving, P.A., Banin, E., and Swaroop, A. (2015). Biology and therapy of inherited retinal degenerative disease: insights from mouse models. Dis. Model. Mech. *8*, 109–129.

2. Mariotti, S.P. (2012). Global Data on Visual Impairments 2010 (World Health Organization).

3. Daiger, S.P. (2017). RetNet: Summaries of Genes and Loci Causing Retinal Diseases. https://sph.uth.edu/retnet/sum-dis.htm.

4. Hartong, D.T., Berson, E.L., and Dryja, T.P. (2006). Retinitis pigmentosa. Lancet *368*, 1795–1809.

5. Adams, M.K., Simpson, J.A., Aung, K.Z., Makeyeva, G.A., Giles, G.G., English, D.R., Hopper, J., Guymer, R.H., Baird, P.N., and Robman, L.D. (2011). Abdominal obesity and age-related macular degeneration. Am. J. Epidemiol. *173*, 1246–1255.

6. Cougnard-Grégoire, A., Delyfer, M.N., Korobelnik, J.F., Rougier, M.B., Malet, F., Le Goff, M., Dartigues, J.F., Colin, J., Barberger-Gateau, P., and Delcourt, C. (2013). Long-term blood pressure and age-related macular degeneration: the ALIENOR study. Invest. Ophthalmol. Vis. Sci. *54*, 1905–1912.

7. Dasari, B., Prasanthi, J.R., Marwarha, G., Singh, B.B., and Ghribi, O. (2011). Cholesterol-enriched diet causes age-related macular degeneration-like pathology in rabbit retina. BMC Ophthalmol. *11*, 22.

8. Fritsche, L.G., Lauer, N., Hartmann, A., Stippa, S., Keilhauer, C.N., Oppermann, M., Pandey, M.K., Köhl, J., Zipfel, P.F., Weber, B.H., and Skerka, C. (2010). An imbalance of human complement regulatory proteins CFHR1, CFHR3 and factor H influences risk for age-related macular degeneration (AMD). Hum. Mol. Genet. *19*, 4694–4704.

9. Hughes, A.E., Orr, N., Esfandiary, H., Diaz-Torres, M., Goodship, T., and Chakravarthy, U. (2006). A common CFH haplotype, with deletion of CFHR1 and CFHR3, is associated with lower risk of age-related macular degeneration. Nat. Genet. *38*, 1173–1177.

10. Thornton, J., Edwards, R., Mitchell, P., Harrison, R.A., Buchan, I., and Kelly, S.P. (2005). Smoking and age-related macular degeneration: a review of association. Eye (Lond.) *19*, 935–944.

11. Bennett, J., Wellman, J., Marshall, K.A., McCague, S., Ashtari, M., DiStefano-Pappas, J., Elci, O.U., Chung, D.C., Sun, J., Wright, J.F., et al. (2016). Safety and durability of effect of contralateral-eye administration of AAV2 gene therapy in patients with childhood-onset blindness caused by RPE65 mutations: a follow-on phase 1 trial. Lancet *388*, 661–672.

12. Choi, V.W., Bigelow, C.E., McGee, T.L., Gujar, A.N., Li, H., Hanks, S.M., Vrouvlianis, J., Maker, M., Leehy, B., Zhang, Y., et al. (2015). AAV-mediated RLBP1 gene therapy improves the rate of dark adaptation in Rlbp1 knockout mice. Mol. Ther. Methods Clin. Dev. *2*, 15022.

13. Georgiadis, A., Duran, Y., Ribeiro, J., Abelleira-Hervas, L., Robbie, S.J., Sünkel-Laing, B., Fourali, S., Gonzalez-Cordero, A., Cristante, E., Michaelides, M., et al. (2016). Development of an optimized AAV2/5 gene therapy vector for Leber congenital amaurosis owing to defects in RPE65. Gene Ther. *23*, 857–862.

14. Ruan, G.X., Barry, E., Yu, D., Lukason, M., Cheng, S.H., and Scaria, A. (2017). CRISPR/Cas9-Mediated Genome Editing as a Therapeutic Approach for Leber Congenital Amaurosis 10. Mol. Ther. *25*, 331–341.

15. Yu, W., Mookherjee, S., Chaitankar, V., Hiriyanna, S., Kim, J.W., Brooks, M., Ataeijannati, Y., Sun, X., Dong, L., Li, T., et al. (2017). Nrl knockdown by AAV-delivered CRISPR/Cas9 prevents retinal degeneration in mice. Nat. Commun. *8*, 14716.

16. Cen, L.P., Liang, J.J., Chen, J.H., Harvey, A.R., Ng, T.K., Zhang, M., Pang, C.P., Cui, Q., and Fan, Y.M. (2017). AAV-mediated transfer of RhoA shRNA and CNTF promotes retinal ganglion cell survival and axon regeneration. Neuroscience *343*, 472–482.

17. Fujita, K., Nishiguchi, K.M., Shiga, Y., and Nakazawa, T. (2017). Spatially and Temporally Regulated *NRF2* Gene Therapy Using *Mcp-1* Promoter in Retinal Ganglion Cell Injury. Mol. Ther. Methods Clin. Dev. *5*, 130–141.

18. Ildefonso, C.J., Jaime, H., Biswal, M.R., Boye, S.E., Li, Q., Hauswirth, W.W., and Lewin, A.S. (2015). Gene therapy with the caspase activation and recruitment domain reduces the ocular inflammatory response. Mol. Ther. *23*, 875–884.

19. Ildefonso, C.J., Jaime, H., Brown, E.E., Iwata, R.L., Ahmed, C.M., Massengill, M.T., Biswal, M.R., Boye, S.E., Hauswirth, W.W., Ash, J.D., et al. (2016). Targeting the Nrf2 Signaling Pathway in the Retina With a Gene-Delivered Secretable and Cell-Penetrating Peptide. Invest. Ophthalmol. Vis. Sci. *57*, 372–386.

20. Ildefonso, C.J., Jaime, H., Rahman, M.M., Li, Q., Boye, S.E., Hauswirth, W.W., Lucas, A.R., McFadden, G., and Lewin, A.S. (2015). Gene delivery of a viral anti-inflammatory protein to combat ocular inflammation. Hum. Gene Ther. *26*, 59–68.

21. LeVaillant, C.J., Sharma, A., Muhling, J., Wheeler, L.P., Cozens, G.S., Hellström, M., Rodger, J., and Harvey, A.R. (2016). Significant changes in endogenous retinal gene expression assessed 1 year after a single intraocular injection of AAV-CNTF or AAV-BDNF. Mol. Ther. Methods Clin. Dev. *3*, 16078.

22. Liang, K.J., Woodard, K.T., Weaver, M.A., Gaylor, J.P., Weiss, E.R., and Samulski, R.J. (2017). AAV-Nrf2 Promotes Protection and Recovery in Animal Models of Oxidative Stress. Mol. Ther. *25*, 765–779.

23. Wassmer, S.J., Leonard, B.C., Coupland, S.G., Baker, A.N., Hamilton, J., Hauswirth, W.W., and Tsilfidis, C. (2017). Overexpression of the X-Linked Inhibitor of Apoptosis Protects Against Retinal Degeneration in a Feline Model of Retinal Detachment. Hum. Gene Ther. *28*, 482–492.

24. Haider, N.B., Olivares, A.M., Flattery, K., Han, Y., Capri, J., and DeAngelis, M.M. (2017). Master Modifier Nr2e3 Rescues Disease and Promotes Retina Homeostasis in Multiple Models of RP. Invest. Ophthalmol. Vis. Sci. *58*, 1575.

25. Lamba, D.A., Gust, J., and Reh, T.A. (2009). Transplantation of human embryonic stem cell-derived photoreceptors restores some visual function in Crx-deficient mice. Cell Stem Cell *4*, 73–79.

26. Lin, B., Koizumi, A., Tanaka, N., Panda, S., and Masland, R.H. (2008). Restoration of visual function in retinal degeneration mice by ectopic expression of melanopsin. Proc. Natl. Acad. Sci. USA *105*, 16009–16014.

27. Kassen, S.C., Thummel, R., Campochiaro, L.A., Harding, M.J., Bennett, N.A., and Hyde, D.R. (2009). CNTF induces photoreceptor neuroprotection and Müller glial cell proliferation through two different signaling pathways in the adult zebrafish retina. Exp. Eye Res. *88*, 1051–1064.

28. Marangoni, D., Vijayasarathy, C., Bush, R.A., Wei, L.L., Wen, R., and Sieving, P.A. (2015). Intravitreal Ciliary Neurotrophic Factor Transiently Improves Cone-Mediated Function in a CNGB3-/- Mouse Model of Achromatopsia. Invest. Ophthalmol. Vis. Sci. *56*, 6810–6822.

29. Ueki, Y., Wang, J., Chollangi, S., and Ash, J.D. (2008). STAT3 activation in photoreceptors by leukemia inhibitory factor is associated with protection from light damage. J. Neurochem. *105*, 784–796.

30. McGill, T.J., Prusky, G.T., Douglas, R.M., Yasumura, D., Matthes, M.T., Nune, G., Donohue-Rolfe, K., Yang, H., Niculescu, D., Hauswirth, W.W., et al. (2007). Intraocular CNTF reduces vision in normal rats in a dose-dependent manner. Invest. Ophthalmol. Vis. Sci. *48*, 5756–5766.

31. Schlichtenbrede, F.C., MacNeil, A., Bainbridge, J.W., Tschernutter, M., Thrasher, A.J., Smith, A.J., and Ali, R.R. (2003). Intraocular gene delivery of ciliary neurotrophic factor results in significant loss of retinal function in normal mice and in the Prph2Rd2/Rd2 model of retinal degeneration. Gene Ther. *10*, 523–527.

32. Xue, W., Cojocaru, R.I., Dudley, V.J., Brooks, M., Swaroop, A., and Sarthy, V.P. (2011). Ciliary neurotrophic factor induces genes associated with inflammation and gliosis in the retina: a gene profiling study of flow-sorted, Müller cells. PLoS ONE *6*, e20326.

33. Iwamoto, M., Björklund, T., Lundberg, C., Kirik, D., and Wandless, T.J. (2010). A general chemical method to regulate protein stability in the mammalian central nervous system. Chem. Biol. *17*, 981–988.

34. Quintino, L., Manfré, G., Wettergren, E.E., Namislo, A., Isaksson, C., and Lundberg, C. (2013). Functional neuroprotection and efficient regulation of GDNF using destabilizing domains in a rodent model of Parkinson's disease. Mol. Ther. *21*, 2169–2180.

35. Tai, K., Quintino, L., Isaksson, C., Gussing, F., and Lundberg, C. (2012). Destabilizing domains mediate reversible transgene expression in the brain. PLoS ONE *7*, e46269.

36. Chu, B.W., Kovary, K.M., Guillaume, J., Chen, L.C., Teruel, M.N., and Wandless, T.J. (2013). The E3 ubiquitin ligase UBE3C enhances proteasome processivity by ubiquitinating partially proteolyzed substrates. J. Biol. Chem. *288*, 34575–34587.

37. Sellmyer, M.A., Chen, L.C., Egeler, E.L., Rakhit, R., and Wandless, T.J. (2012). Intracellular context affects levels of a chemically dependent destabilizing domain. PLoS ONE *7*, e43297.

38. Kay, C.N., Ryals, R.C., Aslanidi, G.V., Min, S.H., Ruan, Q., Sun, J., Dyka, F.M., Kasuga, D., Ayala, A.E., Van Vliet, K., et al. (2013). Targeting photoreceptors via intravitreal delivery using novel, capsid-mutated AAV vectors. PLoS ONE *8*, e62097.

39. Yin, L., Greenberg, K., Hunter, J.J., Dalkara, D., Kolstad, K.D., Masella, B.D., Wolfe, R., Visel, M., Stone, D., Libby, R.T., et al. (2011). Intravitreal injection of AAV2 transduces macaque inner retina. Invest. Ophthalmol. Vis. Sci. *52*, 2775–2783.

40. Thomas, G. (2002). Furin at the cutting edge: from protein traffic to embryogenesis and disease. Nat. Rev. Mol. Cell Biol. *3*, 753–766.

41. Chang, B., Hawes, N.L., Pardue, M.T., German, A.M., Hurd, R.E., Davisson, M.T., Nusinowitz, S., Rengarajan, K., Boyd, A.P., Sidney, S.S., et al. (2007). Two mouse retinal degenerations caused by missense mutations in the beta-subunit of rod cGMP phosphodiesterase gene. Vision Res. *47*, 624–633.

42. Isiegas, C., Marinich-Madzarevich, J.A., Marchena, M., Ruiz, J.M., Cano, M.J., de la Villa, P., Hernández-Sánchez, C., de la Rosa, E.J., and de Pablo, F. (2016). Intravitreal Injection of Proinsulin-Loaded Microspheres Delays Photoreceptor Cell Death and Vision Loss in the rd10 Mouse Model of Retinitis Pigmentosa. Invest. Ophthalmol. Vis. Sci. *57*, 3610–3618.

43. Ly, A., Merl-Pham, J., Priller, M., Gruhn, F., Senninger, N., Ueffing, M., and Hauck, S.M. (2016). Proteomic Profiling Suggests Central Role Of STAT Signaling during Retinal Degeneration in the rd10 Mouse Model. J. Proteome Res. *15*, 1350–1359.

44. Roche, S.L., Wyse-Jackson, A.C., Byrne, A.M., Ruiz-Lopez, A.M., and Cotter, T.G. (2016). Alterations to retinal architecture prior to photoreceptor loss in a mouse model of retinitis pigmentosa. Int. J. Dev. Biol. *60*, 127–139.

45. Sánchez-Vallejo, V., Benlloch-Navarro, S., Trachsel-Moncho, L., López-Pedrajas, R., Almansa, I., Romero, F.J., and Miranda, M. (2016). Alterations in glutamate cysteine ligase content in the retina of two retinitis pigmentosa animal models. Free Radic. Biol. Med. *96*, 245–254.

46. McGill, T.J., Prusky, G.T., Luna, G., LaVail, M.M., Fisher, S.K., and Lewis, G.P. (2012). Optomotor and immunohistochemical changes in the juvenile S334ter rat. Exp. Eye Res. *104*, 65–73.

47. Prusky, G.T., West, P.W., and Douglas, R.M. (2000). Behavioral assessment of visual acuity in mice and rats. Vision Res. *40*, 2201–2209.

48. Penn, J.S., Naash, M.I., and Anderson, R.E. (1987). Effect of light history on retinal antioxidants and light damage susceptibility in the rat. Exp. Eye Res. *44*, 779–788.

49. Gossen, M., and Bujard, H. (1992). Tight control of gene expression in mammalian cells by tetracycline-responsive promoters. Proc. Natl. Acad. Sci. USA *89*, 5547–5551.

50. McGee Sanftner, L.H., Rendahl, K.G., Quiroz, D., Coyne, M., Ladner, M., Manning, W.C., and Flannery, J.G. (2001). Recombinant AAV-mediated delivery of a tet-inducible reporter gene to the rat retina. Mol. Ther. *3*, 688–696.

51. Stieger, K., Le Meur, G., Lasne, F., Weber, M., Deschamps, J.Y., Nivard, D., Mendes-Madeira, A., Provost, N., Martin, L., Moullier, P., and Rolling, F. (2006). Long-term doxycycline-regulated transgene expression in the retina of nonhuman primates following subretinal injection of recombinant AAV vectors. Mol. Ther. *13*, 967–975.

52. Auricchio, A., Rivera, V.M., Clackson, T., O'Connor, E.E., Maguire, A.M., Tolentino, M.J., Bennett, J., and Wilson, J.M. (2002). Pharmacological regulation of protein expression from adeno-associated viral vectors in the eye. Mol. Ther. *6*, 238–242.

53. Naidoo, J., and Young, D. (2012). Gene regulation systems for gene therapy applications in the central nervous system. Neurol. Res. Int. *2012*, 595410.

54. Banaszynski, L.A., Chen, L.C., Maynard-Smith, L.A., Ooi, A.G., and Wandless, T.J. (2006). A rapid, reversible, and tunable method to regulate protein function in living cells using synthetic small molecules. Cell *126*, 995–1004.

55. Le Guiner, C., Stieger, K., Toromanoff, A., Guilbaud, M., Mendes-Madeira, A., Devaux, M., Guigand, L., Cherel, Y., Moullier, P., Rolling, F., and Adjali, O. (2014). Transgene regulation using the tetracycline-inducible TetR-KRAB system after AAV-mediated gene transfer in rodents and nonhuman primates. PLoS ONE *9*, e102538.

56. Chenuaud, P., Larcher, T., Rabinowitz, J.E., Provost, N., Cherel, Y., Casadevall, N., Samulski, R.J., and Moullier, P. (2004). Autoimmune anemia in macaques following erythropoietin gene therapy. Blood *103*, 3303–3304.

57. Favre, D., Blouin, V., Provost, N., Spisek, R., Porrot, F., Bohl, D., Marmé, F., Chérel, Y., Salvetti, A., Hurtrel, B., et al. (2002). Lack of an immune response against the tetracycline-dependent transactivator correlates with long-term doxycycline-regulated transgene expression in nonhuman primates after intramuscular injection of recombinant adeno-associated virus. J. Virol. *76*, 11605–11611.

58. Allocca, M., Di Vicino, U., Petrillo, M., Carlomagno, F., Domenici, L., and Auricchio, A. (2007). Constitutive and AP20187-induced Ret activation in photoreceptors does not protect from light-induced damage. Invest. Ophthalmol. Vis. Sci. *48*, 5199–5206.

59. Trapani, I., Colella, P., Sommella, A., Iodice, C., Cesi, G., de Simone, S., Marrocco, E., Rossi, S., Giunti, M., Palfi, A., et al. (2014). Effective delivery of large genes to the retina by dual AAV vectors. EMBO Mol. Med. *6*, 194–211.

60. Brown, E.J., Albers, M.W., Shin, T.B., Ichikawa, K., Keith, C.T., Lane, W.S., and Schreiber, S.L. (1994). A mammalian protein targeted by G1-arresting rapamycin-receptor complex. Nature *369*, 756–758.

61. Chaveroux, C., Bruhat, A., Carraro, V., Jousse, C., Averous, J., Maurin, A.C., Parry, L., Mesclon, F., Muranishi, Y., Cordelier, P., et al. (2016). Regulating the expression of therapeutic transgenes by controlled intake of dietary essential amino acids. Nat. Biotechnol. *34*, 746–775.

62. Jakobsson, J., Rosenqvist, N., Mårild, K., V Agoston, D., and Lundberg, C. (2006). Evidence for disease-regulated transgene expression in the brain with use of lentiviral vectors. J. Neurosci. Res. *84*, 58–67.

63. Yu, Y., Lowy, M.M., and Elble, R.C. (2016). Tet-On lentiviral transductants lose inducibility when silenced for extended intervals in mammary epithelial cells. Metab. Eng. Commun. *3*, 64–67.

64. Jackson, A.L., Bartz, S.R., Schelter, J., Kobayashi, S.V., Burchard, J., Mao, M., Li, B., Cavet, G., and Linsley, P.S. (2003). Expression profiling reveals off-target gene regulation by RNAi. Nat. Biotechnol. *21*, 635–637.

65. Miyazaki, Y., Imoto, H., Chen, L.C., and Wandless, T.J. (2012). Destabilizing domains derived from the human estrogen receptor. J. Am. Chem. Soc. *134*, 3942–3945.

66. Navarro, R., Chen, L.C., Rakhit, R., and Wandless, T.J. (2016). A Novel Destabilizing Domain Based on a Small-Molecule Dependent Fluorophore. ACS Chem. Biol. *11*, 2101–2104.

67. Wang, E.E., and Prober, C.G. (1983). Ventricular cerebrospinal fluid concentrations of trimethoprim-sulphamethoxazole. J. Antimicrob. Chemother. *11*, 385–389.

68. Drugs.com. (2018). Polymyxin B and trimethoprim ophthalmic, https://www.drugs.com/mtm/polymyxin-b-and-trimethoprim-ophthalmic.html.

69. Reagan-Shaw, S., Nihal, M., and Ahmad, N. (2008). Dose translation from animal to human studies revisited. FASEB J. *22*, 659–661.

70. Nair, A.B., and Jacob, S. (2016). A simple practice guide for dose conversion between animals and human. J. Basic Clin. Pharm. *7*, 27–31.

71. Drugs.com. (2018). Sulfamethoxazole / Trimethoprim Dosage. https://www.drugs.com/dosage/sulfamethoxazole-trimethoprim.html.

72. Nakashima, K., Aoshima, M., Nakashita, T., Hara, M., Otsuki, A., Noma, S., Misawa, M., Otsuka, Y., and Motojima, S. (2017). Low-dose trimethoprim-sulfamethoxazole treatment for pneumocystis pneumonia in non-human immunodeficiency virus-infected immunocompromised patients: A single-center retrospective observational cohort study. J. Microbiol. Immunol. Infect., S1684-1182(17)30147-0.

73. Rungoe, C., Malchau, E.L., Larsen, L.N., and Schroeder, H. (2010). Infections during induction therapy for children with acute lymphoblastic leukemia. the role of sulfamethoxazole-trimethoprim (SMX-TMP) prophylaxis. Pediatr. Blood Cancer *55*, 304–308.

74. Scherwin, J., and Holm, P. (1977). Long-term treatment with sulphamethoxazole/trimethoprim (Bactrim) and nitrofurantoin in chronic urinary tract infections. A controlled clinical trial. Chemotherapy *23*, 282–288.

75. Prasad, V. (2018). Immunotherapy: Tisagenlecleucel - the first approved CAR-T-cell therapy: implications for payers and policy makers. Nat. Rev. Clin. Oncol. *15*, 11–12.

76. Ledford, H. (2017). FDA advisers back gene therapy for rare form of blindness. Nature *550*, 314.

77. Cideciyan, A.V., Jacobson, S.G., Beltran, W.A., Sumaroka, A., Swider, M., Iwabe, S., Roman, A.J., Olivares, M.B., Schwartz, S.B., Komáromy, A.M., et al. (2013). Human retinal gene therapy for Leber congenital amaurosis shows advancing retinal degeneration despite enduring visual improvement. Proc. Natl. Acad. Sci. USA *110*, E517–E525.

78. Jacobson, S.G., Cideciyan, A.V., Ratnakaram, R., Heon, E., Schwartz, S.B., Roman, A.J., Peden, M.C., Aleman, T.S., Boye, S.L., Sumaroka, A., et al. (2012). Gene therapy for leber congenital amaurosis caused by RPE65 mutations: safety and efficacy in 15 children and adults followed up to 3 years. Arch. Ophthalmol. *130*, 9–24.

79. Yao, J., Jia, L., Khan, N., Zheng, Q.D., Moncrief, A., Hauswirth, W.W., Thompson, D.A., and Zacks, D.N. (2012). Caspase inhibition with XIAP as an adjunct to AAV vector gene-replacement therapy: improving efficacy and prolonging the treatment window. PLoS ONE *7*, e37197.

80. West, E.L., Pearson, R.A., Barker, S.E., Luhmann, U.F., Maclaren, R.E., Barber, A.C., Duran, Y., Smith, A.J., Sowden, J.C., and Ali, R.R. (2010). Long-term survival of photoreceptors transplanted into the adult murine neural retina requires immune modulation. Stem Cells *28*, 1997–2007.

81. Hambright, D., Park, K.Y., Brooks, M., McKay, R., Swaroop, A., and Nasonkin, I.O. (2012). Long-term survival and differentiation of retinal neurons derived from human embryonic stem cell lines in un-immunosuppressed mouse retina. Mol. Vis. *18*, 920–936.

82. Burger, C., Gorbatyuk, O.S., Velardo, M.J., Peden, C.S., Williams, P., Zolotukhin, S., Reier, P.J., Mandel, R.J., and Muzyczka, N. (2004). Recombinant AAV viral vectors pseudotyped with viral capsids from serotypes 1, 2, and 5 display differential efficiency and cell tropism after delivery to different regions of the central nervous system. Mol. Ther. *10*, 302–317.

83. Prima, V., Tennant, M., Gorbatyuk, O.S., Muzyczka, N., Scarpace, P.J., and Zolotukhin, S. (2004). Differential modulation of energy balance by leptin, ciliary neurotrophic factor, and leukemia inhibitory factor gene delivery: microarray deoxyribonucleic acid-chip analysis of gene expression. Endocrinology *145*, 2035–2045.

84. Zolotukhin, S., Potter, M., Zolotukhin, I., Sakai, Y., Loiler, S., Fraites, T.J., Jr., Chiodo, V.A., Phillipsberg, T., Muzyczka, N., Hauswirth, W.W., et al. (2002). Production and purification of serotype 1, 2, and 5 recombinant adeno-associated viral vectors. Methods *28*, 158–167.

85. Sarthy, V.P., Brodjian, S.J., Dutt, K., Kennedy, B.N., French, R.P., and Crabb, J.W. (1998). Establishment and characterization of a retinal Müller cell line. Invest. Ophthalmol. Vis. Sci. *39*, 212–216.

YMTHE, Volume *26*

Supplemental Information

A Drug-Tunable Gene Therapy for Broad-Spectrum Protection against Retinal Degeneration

Clayton P. Santiago, Casey J. Keuthan, Sanford L. Boye, Shannon E. Boye, Aisha A. Imam, and John D. Ash

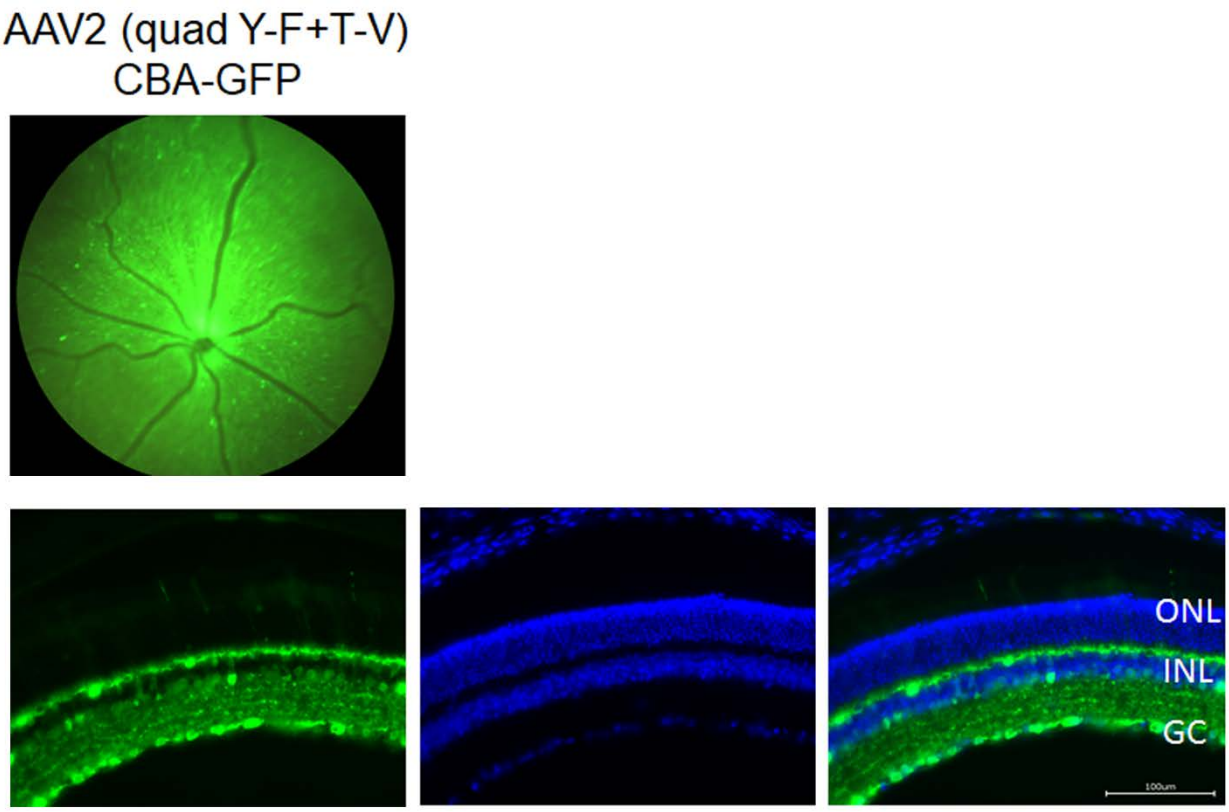

Supplemental Figure 1. Transduction profile of AAV2 (quadY-F+T-V) in the mouse retina. Top: Fundus images of the retina 7 weeks post-injected with AAV2 (quadY-F+T-V) CBA-GFP. The green channel shows the extent of GFP expression in the retina. Bottom: Immunohistochemistry cross section of the same retina showing GFP (green) expression and DAPI nuclei staining (blue). Majority of ganglion cells and some cell in the inner nuclear layer show GFP expression, while expression is only seen in a few photoreceptors in the outer nuclear layer. Images were taken at 40X magnification. White bar indicates 100μm. ONL = Outer nuclear layer, INL = Inner nuclear layer and GC = Ganglion cell layer.

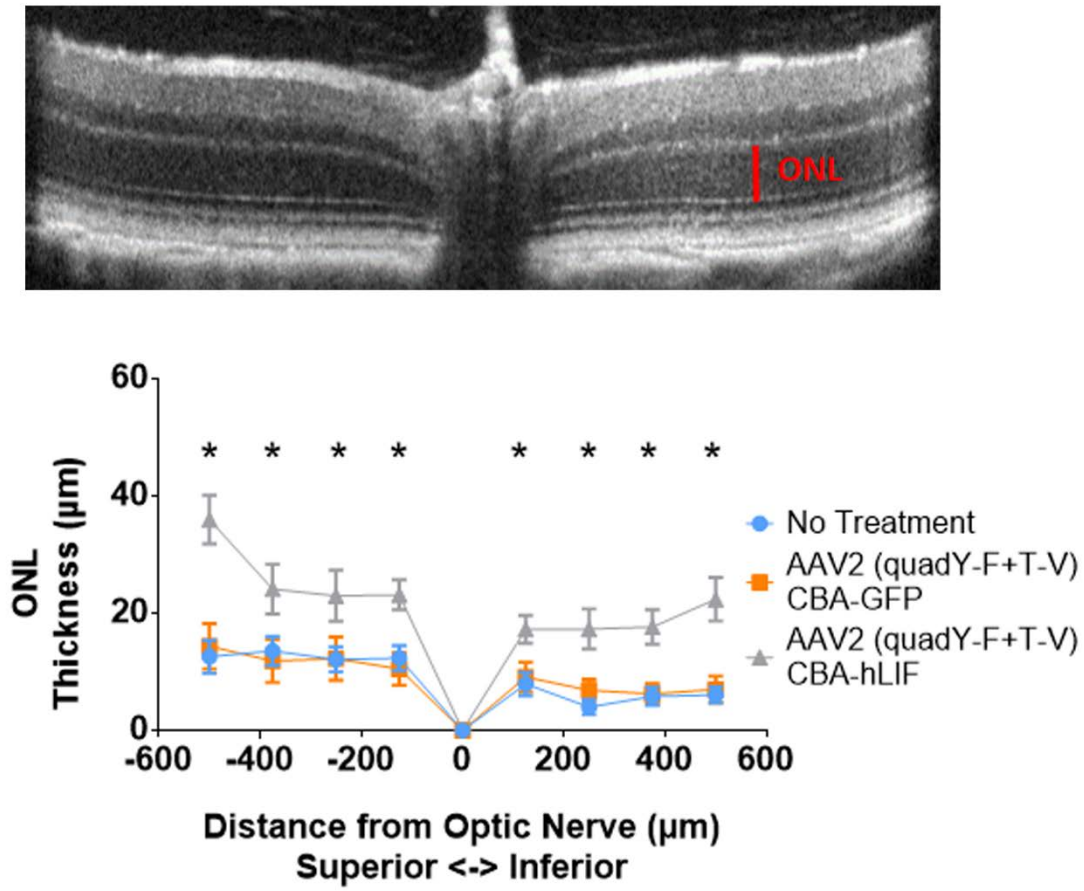

Supplemental Figure 2. AAV delivery of hLIF protects the retina from light damage. Top: Representative OCT image showing the ONL thickness quantification method. Bottom: Spider plot showing the quantification of the ONL thickness of light damaged retinas treated with low titer AAV2 (quad Y-F+T-V) CBA-hLIF. No treatment and AAV2 (quad Y-F+T-V) CBA-GFP injected were used as controls. Groups treated with vectors carrying CBA-hLIF show significant preservation of the ONL compared to controls. Two-way ANOVA with Sidak post-hoc test was performed. n = 8 biological replicates. * indicate $p < 0.05$. Error bars represent SD for each group.

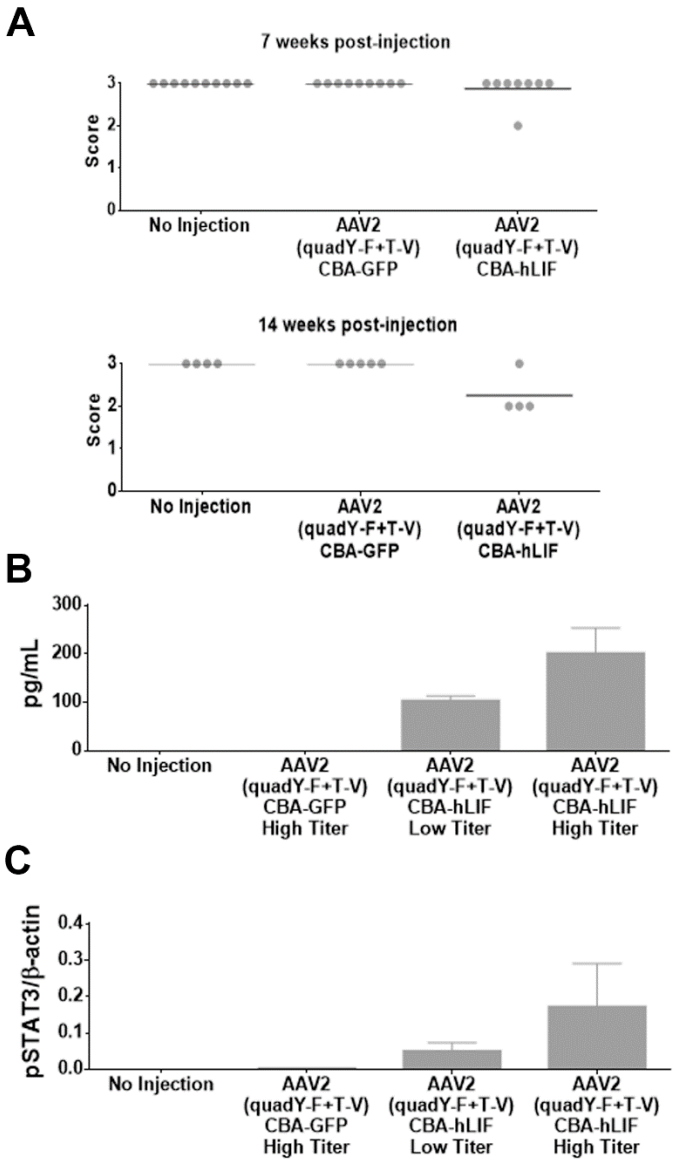

Supplemental Figure 3. Characterization of AAV-hLIF delivery in the mouse retina. (A) Scoring of retinas injected with high titer AAV2 (quadY-F+T-V) CBA-hLIF 7 (top) and 14 (bottom) weeks post-injection. Each filled circle represents one animal (n = 3-10) and the black lines represent the mean for each group. Retinas constitutively expressing LIF had low retinal quality scores. **(B)** Quantification of hLIF in retinas injected with low titer or high titer AAV2 (quadY-F+T-V) CBA-hLIF as determined by ELISA. Higher viral titer delivery led to increased hLIF expression in the retina. **(C)** Immunoblot analysis of pSTAT3 Y705 levels in retinas treated with AAV2 (quadY-F+T-V) CBA-hLIF. Animals treated with the AAV2 (quadY-F+T-V) CBA-hLIF had increased activated STAT3 levels when compared to controls and were greater in high titer-treated groups. For B and C, n = 3-4 biological replicates per group. Error bars represent SD for each group.

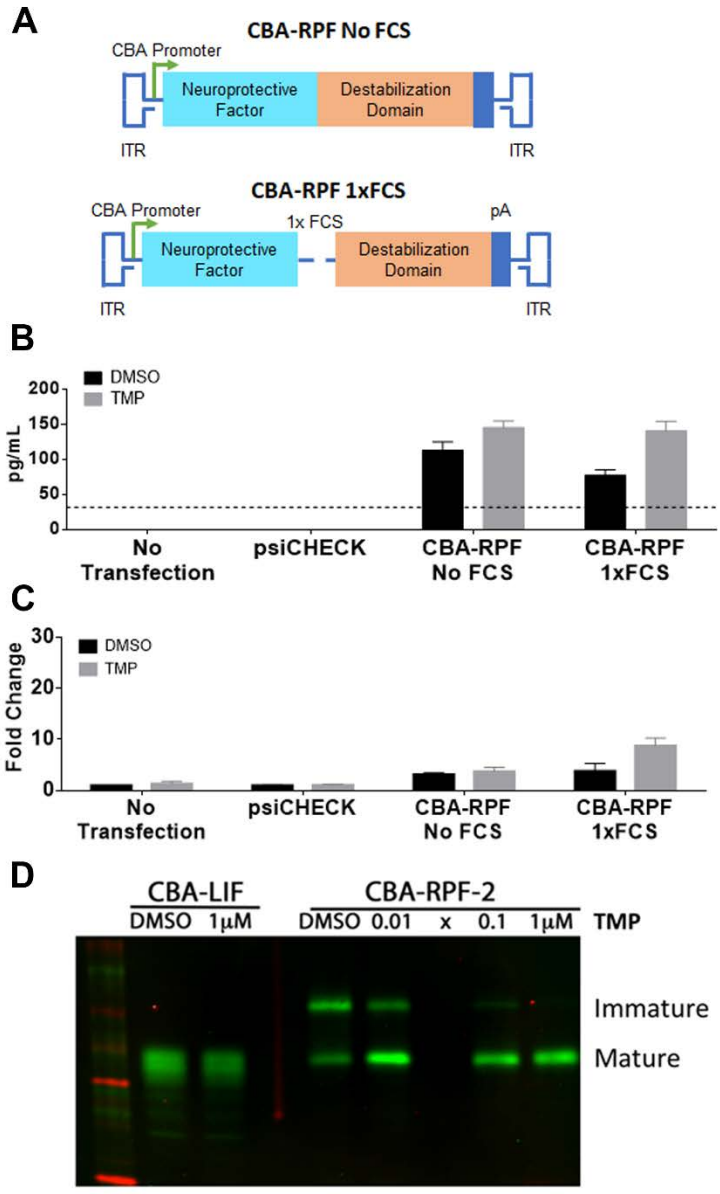

Supplemental Figure 4. Iterations of RPF2 development. (A) Schematics of CBA-RPF iterations with no or one furin cleavage site (FCS). **(B)** Levels of cytokine secreted by rMC-1 transfected cells into the conditioned media detected by ELISA. Dotted line indicates the limit of detection for the assay (32pg/ml). **(C)** Quantification of pSTAT3 in rMC-1 cells treated with conditioned media. The initial iterations of RPF2 were not efficiently regulated by TMP. Additionally, these iterations resulted in low STAT3 activation. For B and C, n = 3 biological replicates. Error bars represent SD for each group. **(D)** Dose-dependent stabilization and maturation of RPF2 by TMP in transfected rMC-1 cells by immunoblot. Increased stabilization and processing of RPF2 to its mature form (lower band) is observed at higher TMP concentration treatments compared to DMSO treatment.

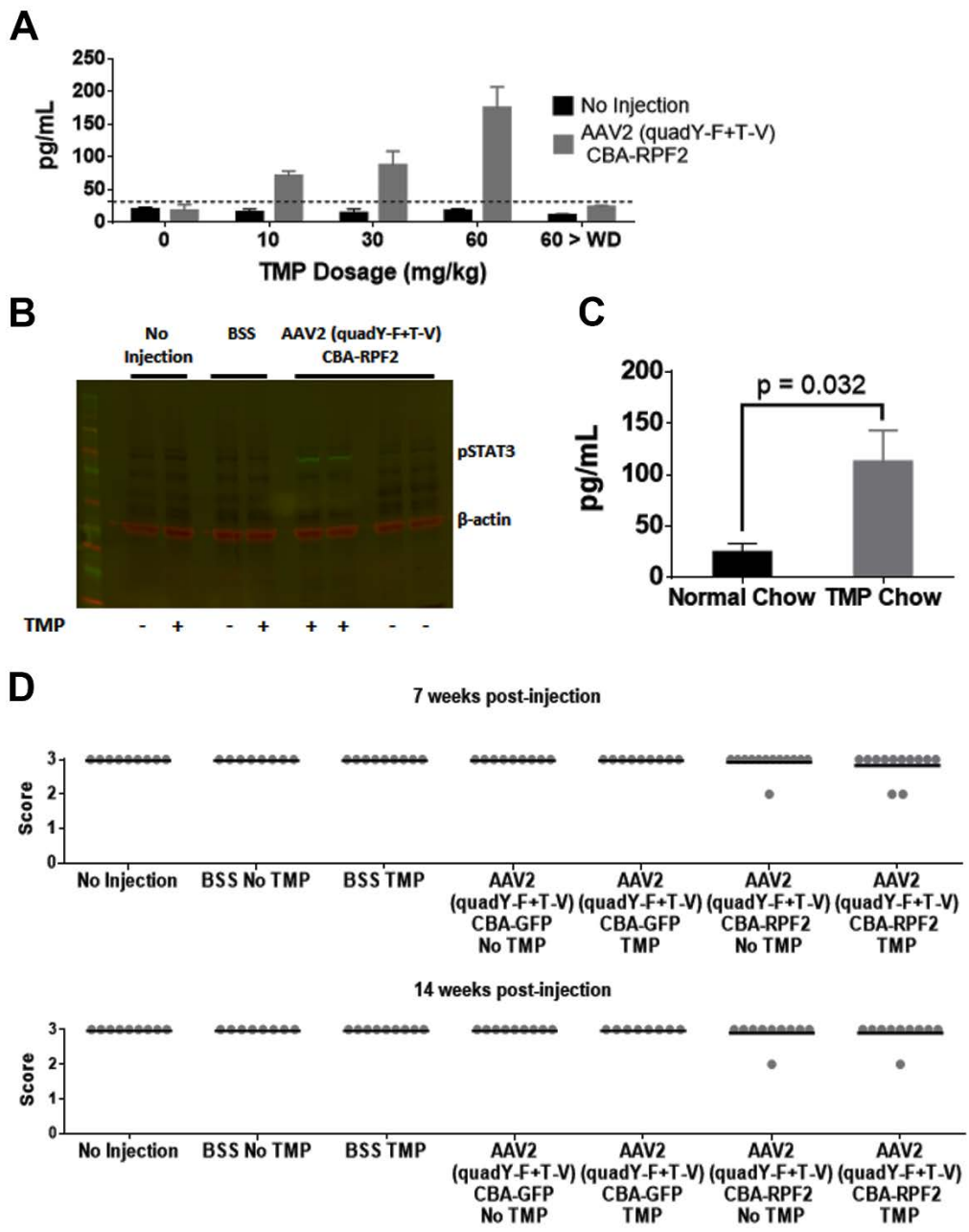

Supplemental Figure 5. Characterization of RPF2 *in vivo.* (A) ELISA levels of RPF2 in the retinal lysates of animals injected with high titer AAV2 (quadY-F+T-V) CBA-RPF2 at varying concentrations of TMP. RPF2 stabilization increased in a dose-dependent manner and was reversible after TMP withdrawal. These changes were not observed in non-injected mice. n = 2 biological replicates for the no injection group and 4 biological replicates for AAV2 (quadY-F+T-V) CBA-RPF2. Error bars represent SD for each group. **(B)** Immunoblot showing STAT3 activation in retinas treated with AAV2 (quadY-F+T-V) CBA-RPF2 with and without TMP. Activation of STAT3 is only observed in RPF2-treated retinas following TMP treatment. **(C)** Stabilization of RPF2 as detected by ELISA after one week of oral TMP administration. AAV2

(quadY-F+T-V) CBA-RPF2 injected animals fed the TMP diet for 7 days show significant stabilization of RPF2 in the retina. Student's t-test with Holm-Sidak post-hoc test was performed; n = 4 biological replicates and error bars represent SD for each group. **(D)** Scoring of retinas injected with high titer AAV2 (quadY-F+T-V) 7 (top) and 14 (bottom) weeks post-injection. Each filled circle represents one animal (n = 9-14) and the black lines represent the mean for each group. Animals injected with RPF2 did now show any significant long-term retinal adverse effects when compared to controls.

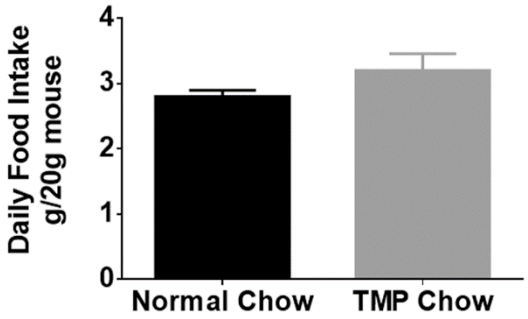

Supplemental Figure 6. TMP diet did not alter eating habits of the animal. Food intake and mouse weight was measured daily for 7 days for animals on normal and TMP supplemented chow. The TMP diet did not lead to any feeding behavior changes compared to controls. Error bars represent SD for each group. n = 4 biological replicates per group. Student's t-test was performed but no significance between the two groups was observed.

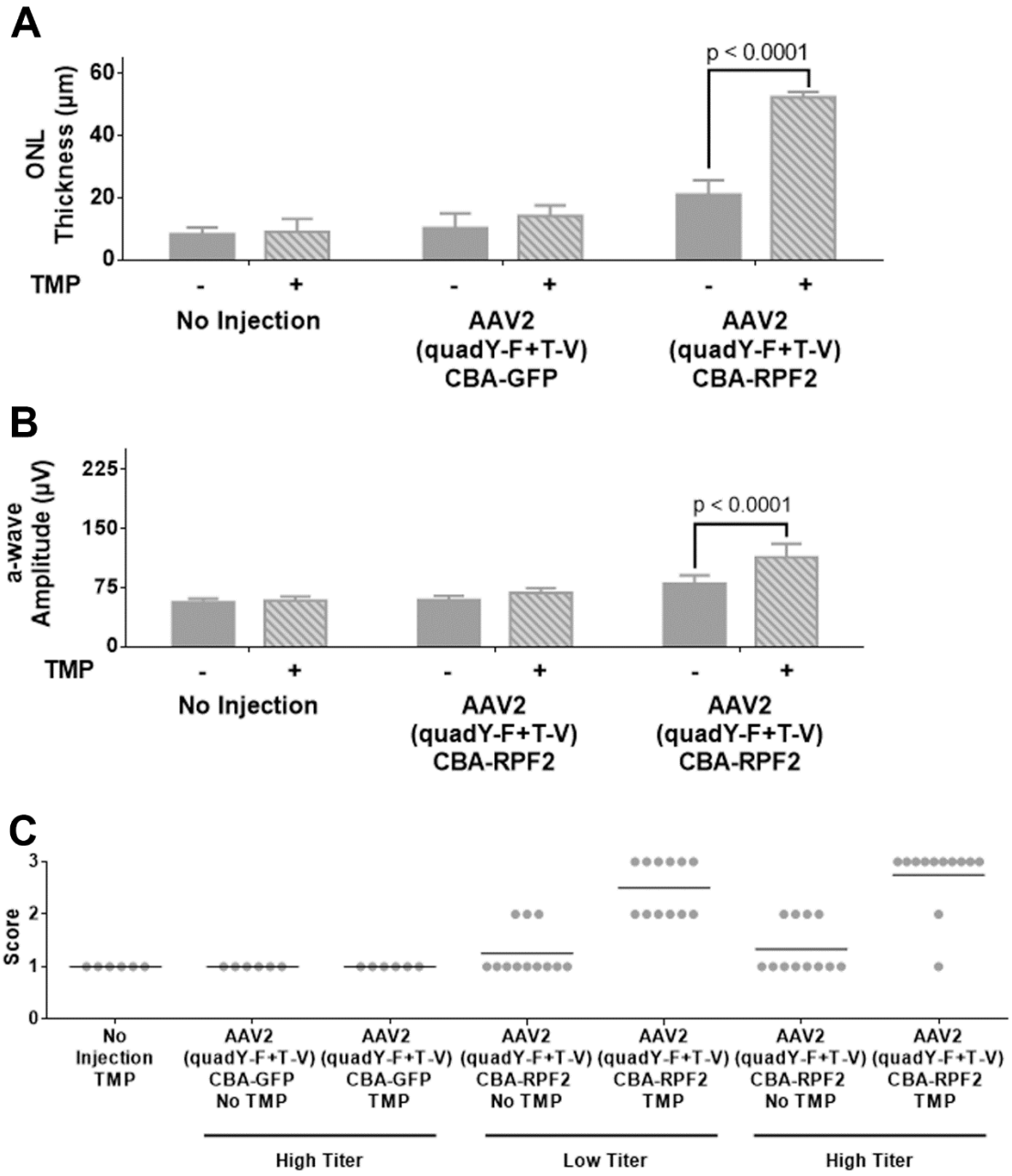

Supplemental Figure 7. High titer AAV2 (quadY-F+T-V) CBA-RPF2-injected retinas showed greater retinal preservation after bright light exposure as compared to low titer counterparts. (A) Averaged thickness of the retinal outer nuclear layer and **(B)** retinal function by ERG after RPF2 stabilization in high titer-treated animals. Two-way ANOVA with Sidak post-hoc test was performed for A-B; n = 6-12 biological replicates per group. Error bars represent SD for each group. **(C)** Retinal scoring of low titer and high titer AAV-RPF2-treated after light damage. Treated animals showed less signs of edema, rosette formation and infiltrating immune cells compared to the control groups. n = 6-12 biological replicates per group.

Plasmid Name	**Promoter**	**Protein expressed**	**Use**
pTR-UF11	chicken beta-actin	Green Fluorescent Protein	To create the AAV2 (quadY-F+T-V) CBA-GFP for animal studies
pTR-CBA-hLIF	chicken beta-actin	human Leukemia Inhibitory Factor	To overexpress hLIF in cell culture and create the AAV2 (quadY-F+T-V) CBA-hLIF for animal studies.
pTR-CBA-RPF2	chicken beta-actin	Retinal Protective Factor 2	To overexpress RPF2 in cell culture and create the AAV2 (quadY-F+T-V) CBA-RPF2 for animal studies.
psiCHECK (Promega Corporation)	SV40 early enhancer/promoter	*Renilla* luciferase	To overexpress luciferase in cell culture as a negative control

Supplemental Table 1. Plasmids used in this study

Name	Company	Catalog No.	Species raised	Use
Biotin hLIF	R&D Systems	BAF250	Goat	0.3µg/ml Detection for ELISA/1:500 dilution Immunoblots
hLIF	R&D Systems	AF-250-NA	Goat	3µg/ml Capture for ELISA
Streptavidin-HRP	R&D Systems	DY998		1:200 dilution Detection signal for ELISA
pSTAT3	Cell Signaling	9145L	Rabbit	1:2,000 dilution Immunoblots
beta actin	Abcam	ab6276	Mouse	1:10,000 dilution Immunoblots
Streptavidin-800CW	Li-Cor	926-32230		1:5,000 dilution Immunoblots
anti-mouse IRDye 680RD	Li-Cor	926-68170	Goat	1:10,000 dilution Immunoblots
anti-rabbit IRDye 800CW	Li-Cor	925-32211	Goat	1:10,000 dilution Immunoblots
s-opsin	Santa Cruz	sc-14363	Goat	1:300 dilution Immunohistochemistry
m-opsin	EMD Millipore	AB5405	Rabbit	1:300 dilution Immunohistochemistry
anti-goat Alexa Fluor 488	Life Technologies	A21206	Donkey	1:500 dilution Immunohistochemistry
anti-rabbit Alexa Fluor 488	Life Technologies	A11055	Donkey	1:500 dilution Immunohistochemistry

Supplemental Table 2. Antibodies used in this study